Dynamic Model of an Industrial Steam Reformer and Its Use for Multiobjective Optimization

Anjana D. Nandasana,[†] Ajay K. Ray,[‡] and Santosh K. Gupta*[,†]

Department of Chemical Engineering, Indian Institute of Technology, Kanpur 208016, India, and Department of Chemical and Environmental Engineering, National University of Singapore, 10, Kent Ridge Crescent, Singapore 119260

An industrial side-fired steam reformer in a hydrogen plant is simulated under dynamic conditions. A rigorous model with verified reaction kinetics is used. This model incorporates aspects of heat transfer in the furnace and diffusion inside the catalyst pellet. The dynamic model is used to study the effects of a few (planned) disturbances that reduce the production of both hydrogen and steam and adversely influence the safety of the plant if corrective control action is not taken in time. The operation of the steam reformer is simulated in the presence of three idealized disturbances in (1) the inlet feed temperature, (2) the inlet feed rate of natural gas, and (3) the furnace gas temperature. The model is then used to obtain optimal operating conditions required to negate the effects of two disturbances using several control or decision variables. Two objective functions are minimized simultaneously: the cumulative (integrated over time) deviation of the flow rate of hydrogen and the cumulative deviation of the steam flow rate. The elitist nondominated sorting genetic algorithm NSGA-II is used to obtain solutions of this multiobjective optimization problem. Nondominating Pareto-optimal solutions are obtained.

Introduction

Steam reforming of hydrocarbons is an economical method of producing synthesis gas and generating hydrogen. The former is the feedstock for the synthesis of ammonia, methanol, etc., and the latter is an environmentally clean fuel.[1] Steam reforming plants also produce considerable amounts of exportable steam. The process flow sheet of a typical plant is shown in Figure 1. A hydrocarbon stream, assumed to be essentially methane (with CO_2 and N_2 impurities) in this study, is desulfurized and preheated. This stream is mixed with appropriate quantities of steam and recycled hydrogen (both from the *plant*) and fed to the first reactor (called the reformer). The following catalytic reactions take place in this reactor

Reforming: $CH_4 + H_2O \rightleftharpoons CO + 3H_2$

$$\Delta H_r = 8.623 \times 10^5 \text{ kJ/kmol} \quad (1)$$

Shift: $CO + H_2O \rightleftharpoons CO_2 + H_2$

$$\Delta H_r = -1.7196 \times 10^5 \text{ kJ/kmol} \quad (2)$$

Reforming: $CH_4 + 2H_2O \rightleftharpoons CO_2 + 4H_2$

$$\Delta H_r = 6.904 \times 10^5 \text{ kJ/kmol} \quad (3)$$

The gas exiting the reformer, rich in CO and H_2, exchanges heat with the boiler feedwater to generate very high pressure (VHP) steam. The cooled process gas is then fed to a two-stage adiabatic shift converter, where CO is converted into CO_2 and additional hydrogen. Hydrogen is separated from the exit gas in a pressure-swing adsorption (PSA) unit.

The reforming reactions (eqs 1 and 3) are strongly endothermic in nature and require large energy inputs. Increasing energy costs and competition require that reforming plants be operated optimally, both under steady-state conditions and in the presence of unplanned disturbances. The effects of these disturbances need to be negated by advanced model-based process control strategies. A good dynamic model is a prerequisite for this. The development and application of such a model-based control strategy is the main focus of the present study.

Several studies[2−6] have been reported in the open literature on the steady-state modeling, simulation, kinetics, optimization, and control of steam reformers. These have been reviewed by Elnashaie and Elshishini[2] and Rajesh et al.[6] Elnashaie and Elshishini[7] also presented an elaborate study on the dynamic modeling of gas−solid catalytic reactors in general but did not study industrial reformers in detail. Alatiqi and coworkers[8−12] reported some work on the dynamic modeling and simulation of industrial steam reformers under load disturbances and validated their simulation results with actual plant data. However, they did not provide complete information on their approach for proprietary reasons. They used different control methods to minimize the effects of disturbances. Their dynamic model uses a simplified overall reaction rate expression rather than eqs 1−3. In addition, the reaction-cum-diffusion of the several molecular species present inside the porous catalyst is not considered separately. Kvamsdal et al.[13] also carried out the dynamic simulation of industrial steam reformers in the presence of sudden stoppages (tripping) of the feed gas flow and of the steam supply. They used the pseudo-homogeneous kinetic model of Xu and Froment.[3] Again, these workers did not provide complete details on the reactor. There is, thus, a definite need for the development of a dynamic model based on first principles, with complete

* To whom correspondence should be addressed. E-mail: skgupta@iitk.ac.in. Fax: 91-512-590104.
[†] Indian Institute of Technology.
[‡] National University of Singapore.

10.1021/ie0209576 CCC: $25.00
Published on Web 07/23/2003

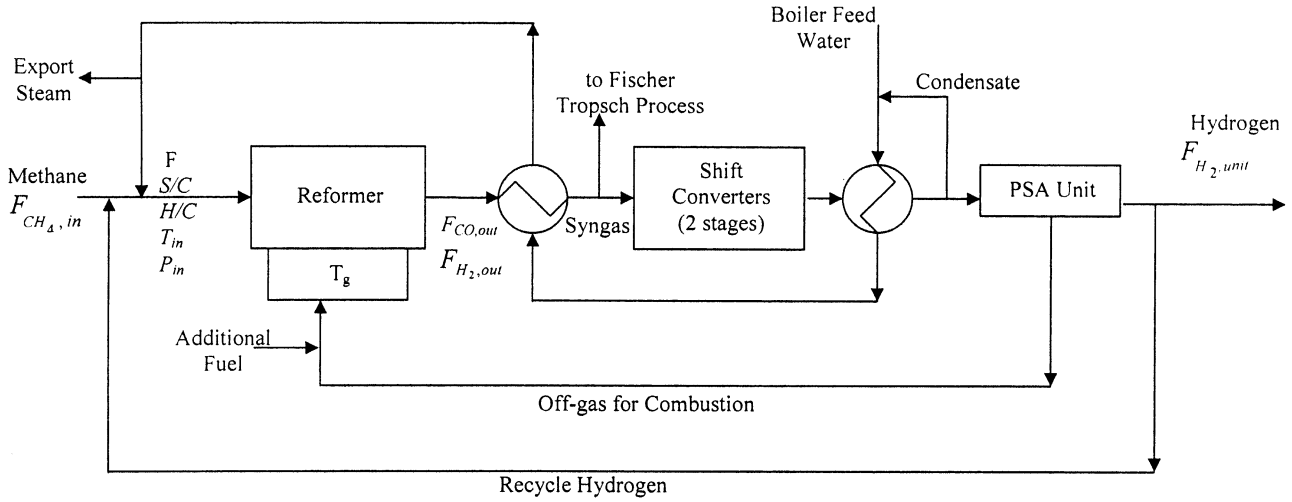

Figure 1. Process flow diagram of the steam reforming plant using natural gas feed.

details provided. Such fundamental models can also be used for off-line optimization purposes to obtain optimal control strategies required to negate the effects of a number of idealized disturbances. A file of such strategies (a few of which are obtained here) would be of immense use for the optimal operation of these plants. It should be mentioned here that the detailed model developed here for the steam reformer is somewhat similar to that for packed-bed adsorbers,[14] in which no reactions take place.

Formulation

The steady-state model[6] of the reformer is modified in this study to apply to transient conditions. The concentrations, $C_i(Z,t)$, and the temperature, $T(Z,t)$, of the gas phase (outside the solid) are functions of both the axial location, Z, and the time, t. It is assumed[2,7] that there are no radial gradients in the gas phase. The equation for $C_i(Z,t)$ can be written,[15] for a semidifferential control volume of length δZ, as

$$\frac{\partial}{\partial Z}(v_l C_i) = \epsilon_b \frac{\partial C_i}{\partial t} + \rho_b \eta_i R_i, \quad i = CH_4, H_2O, CO_2, CO, H_2 \quad (4)$$

Here, v_l is the superficial velocity of the gas; ϵ_b is the void fraction in the catalyst bed (outside the porous solids); ρ_b is the density of the catalyst bed (including the void in the bed and the pores in the catalyst); R_i is the net rate of consumption of the ith species because of the three reactions, which is related to r_i, the (net) forward rate of the ith reaction (eqs 1−3), at the conditions just outside the catalyst particle, through the stoichiometric coefficients $\sigma_{i,k}$; and η_i is the effectiveness factor for the ith reaction.[6] No accumulation term corresponding to the solid is necessary in this equation, as the balance is on the gas alone.

The most general form of the energy balance equation[15] would make the problem computationally intense and would require separate equations for the gas and solid phases. In such a model, the temperature of the solid phase, $T_s(Z,t,l)$, would depend on Z and t as well as the internal location, l. At the solid boundary, this temperature would be related to the local gas-phase temperature, $T(Z,t)$, through a gas−film resistance model. Simplifying assumptions are needed to obtain a model that is useful for optimization and control. It is known[2,4,16] that the thermal conductivity of the catalyst pellet is quite high (low Prater number). Also, the resistance of the gas film surrounding the catalyst particles is small.[16] Under these conditions, we can assume that the entire catalyst particle attains the temperature, $T(Z,t)$, of the gas phase (at axial position Z and time t) instantly. Villadsen and Michelsen[17] and Elnashaie and Elshishini[2] mention that this is a reasonable approximation to make. We can then write the simplified energy balance equation for the semidifferential control volume (gas plus solid) of length δZ as

$$\frac{\partial}{\partial Z}(GC_{p,g}A_cT) = \pi d_i U(T_{w,i} - T) - (\{C_{p,s}\rho_b + [\epsilon_b + (1-\epsilon_b)\epsilon_c]\rho_g C_{p,g}\}A_c)\frac{\partial T}{\partial t} + A_c\sum_{i=I}^{III}(-\Delta H_i)\eta_i r_i \rho_b \quad (5)$$

In eq 5, G ($\equiv \rho_g v_l$) is the mass velocity of the gas; ϵ_c is the volume fraction of the pores inside the catalyst particles, ρ_s and ρ_g are the densities of the porous catalyst (kilograms of solid per cubic meter of porous catalyst particles) and of the pure gas, respectively; U is the film heat-transfer coefficient on the inside of the tube surface (sum of the effects of heat transfer to the gas and to the solid); $C_{p,g}$ and $C_{p,s}$ are the heat capacities of the pure gas mixture (in the voids) and of the solid catalyst (without pores), respectively; $T_{w,i}$ is the temperature at the inner tube wall; and ΔH_i is the heat of reaction of the ith reaction. Equation 5 can easily be deduced from eqs e and f (page 492) of Froment and Bischoff,[15] using these assumptions. It would be interesting to compare the results obtained from the simplified model developed here with those obtained using a more rigorous model for $T_s(Z,t,l)$, when the latter becomes available (work is in progress along these lines).

The following initial conditions (ICs) can be used with eqs 4 and 5

$$C_i(Z,t=0) = C_i^{SS}(Z), \quad 0 \le Z \le L \quad (6a)$$

$$T(Z,t=0) = T_i^{SS}(Z), \quad 0 \le Z \le L \quad (6b)$$

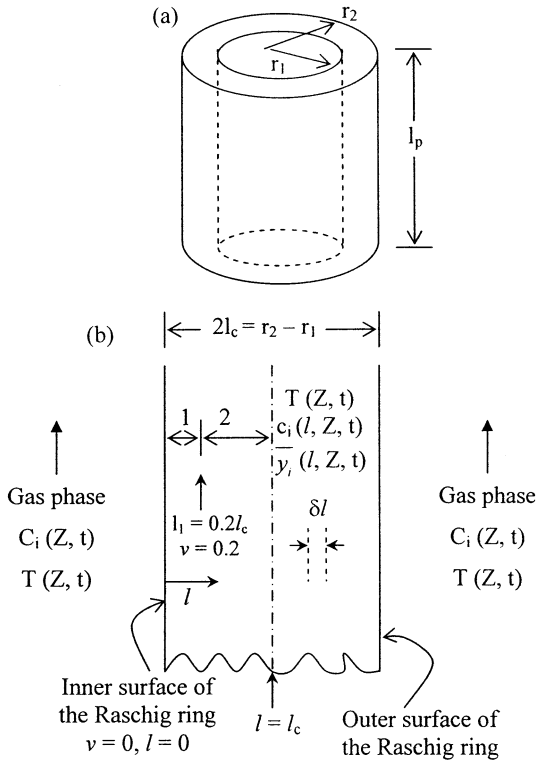

Figure 2. (a) Sketch of the catalyst pellet (Raschig ring). (b) Notation used for the reaction−diffusion problem.

Here, C_i^{SS} and T^{SS} are the profiles that can be obtained using the steady-state (SS) code of Rajesh et al.[6] It is assumed that the reformer is operating at steady state for $t \le 0$ and that a disturbance is introduced at $t = 0$.

Because most of the gradient in the catalyst particle exists in thin layers near the two faces of the Raschig ring catalyst particle, the latter can be assumed to have a slab geometry,[6] i.e., it can be sliced along the length and opened up to give an equivalent slab geometry having a cross-sectional area A_p [$\equiv \pi(r_1 + r_2)l_p$] and thickness $2l_c$ ($= r_2 - r_1$) (see Figure 2). The simplified model II of Elnashaie and Elshishini[2] gives the following equations at time t for the intrapellet concentrations, c_i

$$\frac{d}{dl}(N_i A_p) = A_p \rho_s \sum_{k=I}^{III} \sigma_{i,k} r_k, \quad i = CH_4, H_2O \qquad (7a)$$

$$N_{H_2} = -N_{H_2O} - 2N_{CH_4} \qquad (7b)$$

$$N_{CO} = N_{H_2O} - 2N_{CH_4} \qquad (7c)$$

$$N_{CO_2} = -N_{H_2O} + N_{CH_4} \qquad (7d)$$

$$N_i = -D_i^e \frac{dc_i}{dl}, \quad i = CH_4, H_2O, CO, CO_2, H_2 \qquad (7e)$$

with the following boundary conditions (BCs) at $l = 0$ and $l = l_c$

$$c_i(l=0,Z,t) = C_i(Z,t), \quad i = CH_4, H_2O, CO, CO_2, H_2$$

$$N_i(l=l_c,Z,t) = 0, \quad i = CH_4, H_2O, CO, CO_2, H_2 \qquad (8)$$

In the above equations, N_i is the molar flux of component i at any location l ($0 \le l \le l_c$) inside the catalyst slab, and D_i^e is the effective diffusivity of component i in the catalyst.[2] r_k is the net forward rate of the kth reaction (k = I−III for eqs 1−3, respectively) at any l and t, and $\sigma_{i,k}$ is the stoichiometric coefficient of the ith component participating in the kth reaction. The concentrations of CO, CO_2, and H_2 (and N_2) inside the catalyst at any location l and time t are evaluated using stoichiometry.[6] The complete set of model equations is given in the appendix. The list of model parameters used, as well as the details of the industrial reformer and the initial operating conditions, are given in Table 1.[2,4,6,18,19] The correlations for the estimation of the effective diffusivity are taken from Elnashaie and Elshishini,[2,6] and the correlations for the specific heat, viscosity, and thermal conductivity are taken from[6] the HYSYS Process (version 1.5) code.

Table 1. Model Parameters for the Industrial Steam Reformer[2,4,6,17,18]

model parameter	value/specification	ref
	reformer data	
heated length of reformer tube, L	11.95 m	2
inside diameter of reformer tubes, d_i	0.0795 m	2
outside diameter of reformer tubes, d_o	0.102 m	2
ratio of reformer tube pitch to diameter	2.4	2
number of tubes	176	2
refractor surface area, A_{ref}	1164 m^2	2
number of burners, N_b	112	2
flame surface area, A_f	0.01 m^2	6
	catalyst data	
catalyst shape	Raschig ring	2
catalyst pellet dimension	16 × 6 × 16 mm	2
pellet porosity, ϵ_c	0.51963	2
pellet sphericity, ϕ_s	0.6563	2
pellet equivalent diameter, D_p	17.4131 mm	2
pellet tortuosity, τ	2.74	2
solid catalyst density, ρ_s	2396.965 kg/m^3	calcd from refs 2, 4
mean pore radius	80.0 Å	2
pellet characteristic length, l_c	1.948 mm	2
catalyst bed density, ρ_b	946.8 kg/m^3	2
catalyst bed void fraction, ϵ_b	0.605	17
	other data	
carbon dioxide-to-methane ratio, D/C	0.091	2
nitrogen-to-methane ratio, N/C	0.021	2
emissivity of flames, ξ_f	0.1	2
emissivity of furnace gases, ξ_g	0.1	2
emissivity of reformer tubes, ξ_t	0.95	18
adiabatic flame temperature, T_f	2200 K	6
tube thermal conductivity, k_w	10.738 + 0.0242T_w W/(m K)	18
no. of collocation points, $M + 2$	10	this work
active fraction, a	0.2	2
k_I, K_I, k_{II}, K_{II}, k_{III}, K_{III}, ΔH_i	−	2, 6
other properties	−	6
	operating conditions at SS1	
$F_{CH_4,in}$	593.564 kmol/h	6
T_g	1625 K	6
S/C	4.8	6
H/C	0.34	6
P_{in}	2548.8 kPa	6
T_{in}	841.7 K	6

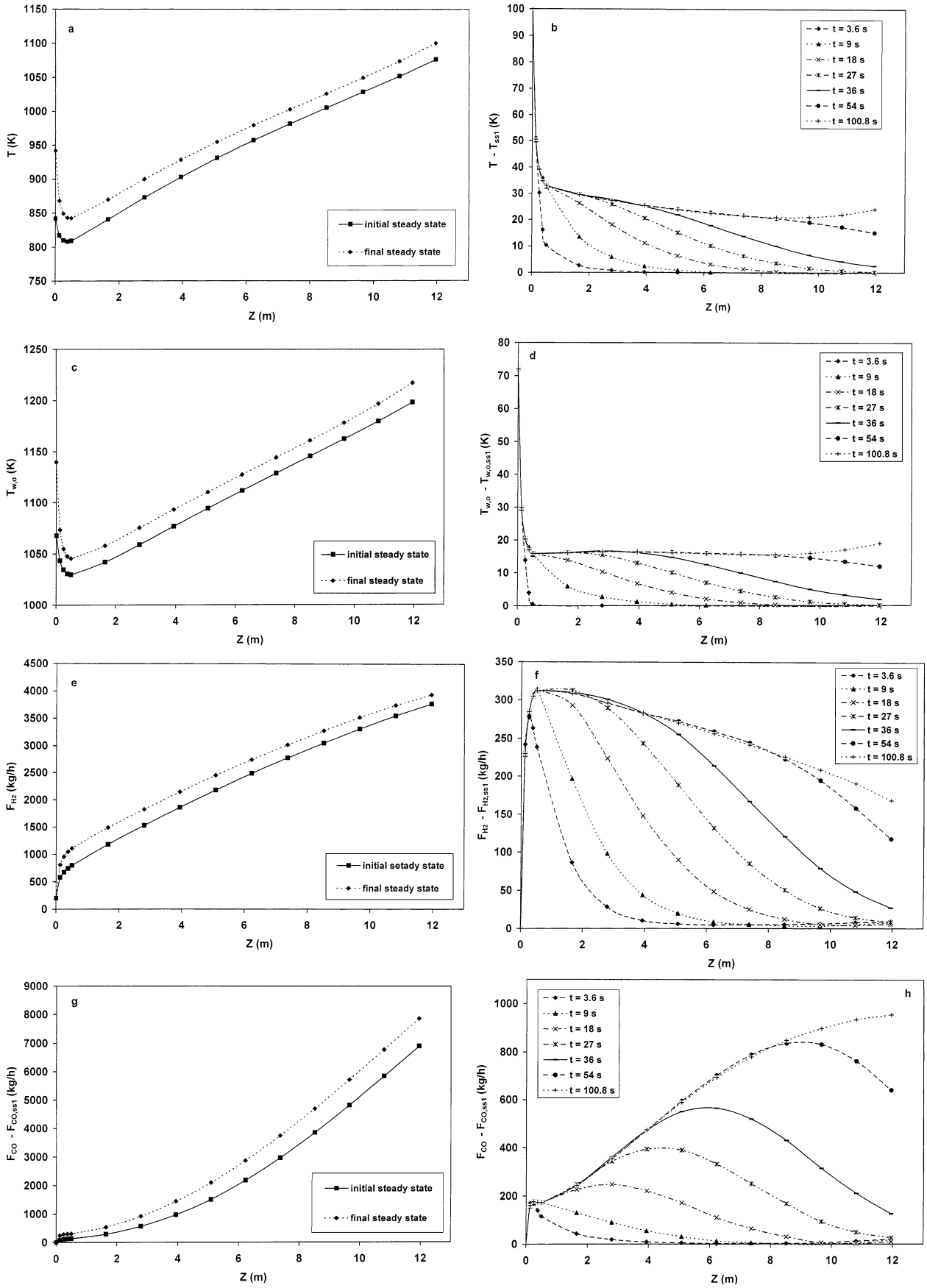

Figure 3. Axial profiles of different variables at the initial and final steady states and the deviations of these variables from their initial steady-state values at different times for the first simulation problem (step increase in the inlet feed temperature).

The profiles, $c_i(l,Z,t)$, and the effectiveness factors, η_i, are evaluated[6] using the method of orthogonal collocation on finite elements (OCFE).[16,20,21] The region $0 \leq l \leq l_c$ is divided into two finite elements[6] extending over $0 \leq v \leq 0.2$ (outer region) and $0.2 \leq v \leq 1$ (inner region), where $v \equiv l/l_c$. It is assumed that all fluxes are zero at

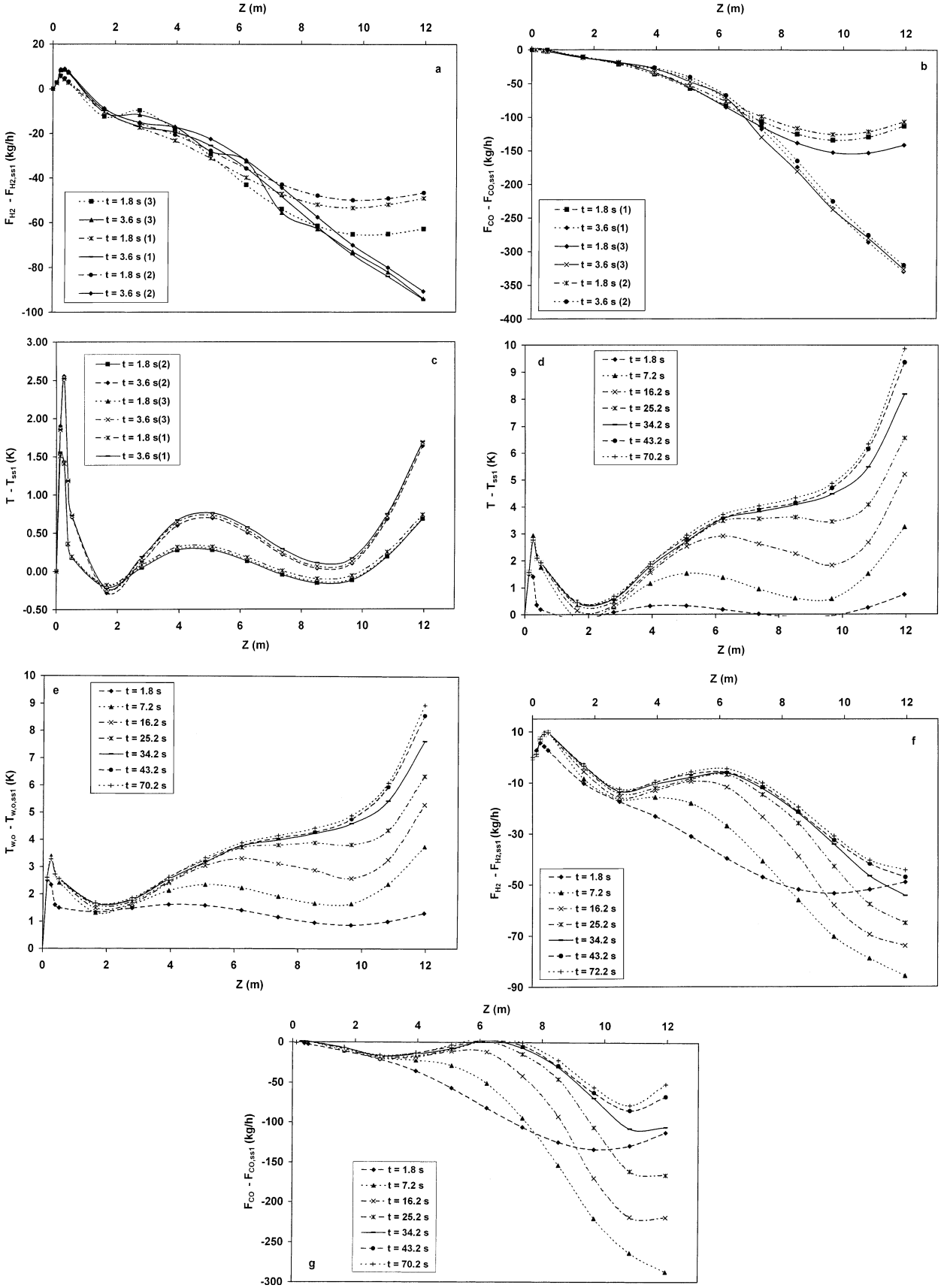

Figure 4. Axial profiles of different variables at the initial and final steady states and the deviations of these variables from their initial steady-state values at different times for the second simulation problem (step decrease in the inlet flow rate of natural gas). Approach numbers (1, 2, and 3) are indicated.

$\nu = 0.2$. This implies that, in the inner region of the catalyst slab, the reactions are at (instantaneous local) equilibrium. There are a total of 10 orthogonal collocation (OC) points (including two at the boundaries of the element) in the outer finite element, where most of the concentration changes take place.

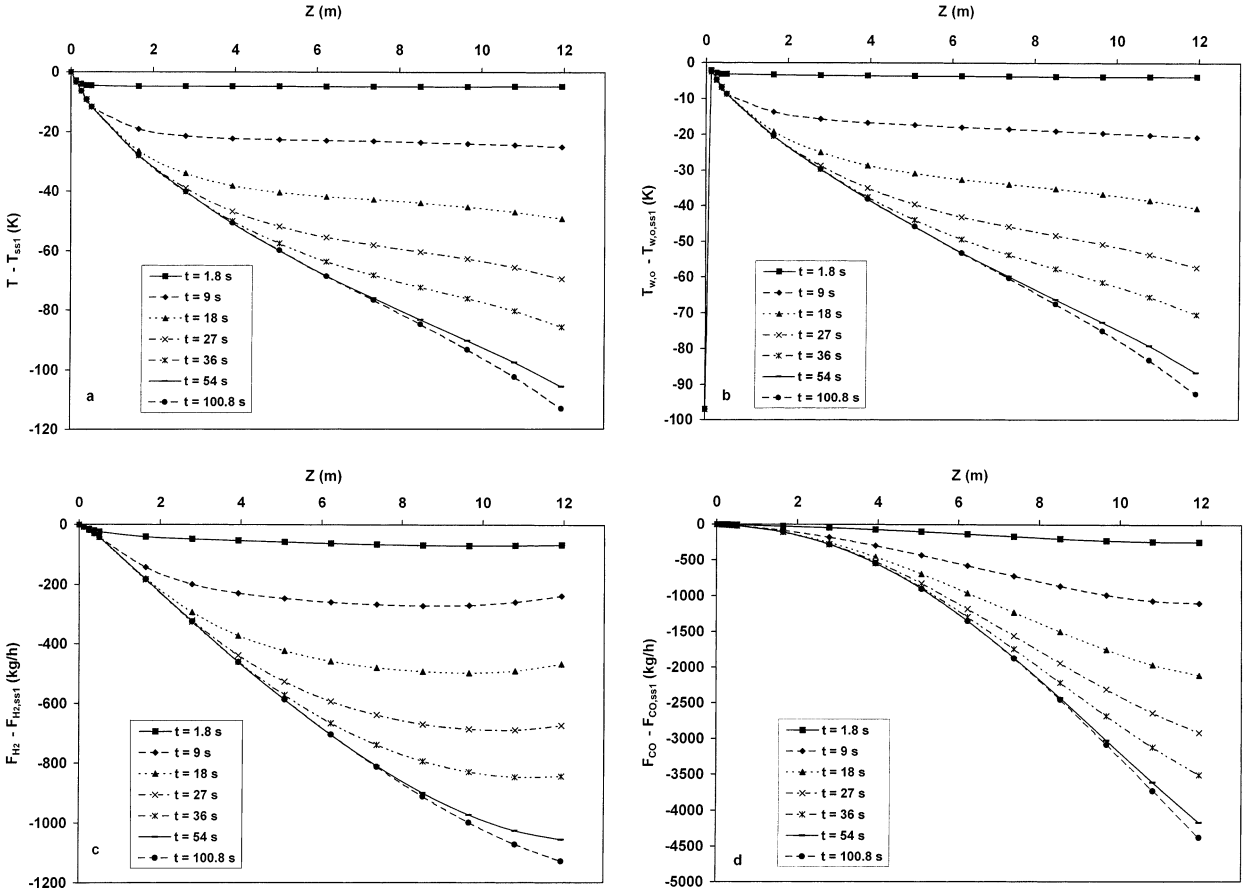

Figure 5. Axial profiles of different variables at the initial and final steady states and the deviations of these variables from their initial steady-state values at different times for the third simulation problem (step decrease in the furnace gas temperature).

The PDEs characterizing the gas phase are converted into ODEs using the finite difference method (the method of lines) with unequal spacing of the grid points [the finite difference equations[21] used are accurate to $O(Z^2)$]. The region $0 \le Z \le 0.5$ m, which encompasses sharp changes in the variables, is divided into six equally spaced grid points (two at $Z = 0$ and 0.5 m). The remaining 11.45 m of the reactor[2,6] is divided into 10 equally spaced grid points. The first point in $0.5 \le Z \le 11.95$ m is the same as the last point in $0 \le Z \le 0.5$ m. The resulting set of ODEs (in t) is solved with the code D02EJF from the NAG library for the integration of stiff ordinary differential equations using Gear's technique.[20,21] We use the C05NCF subroutine of the NAG library to solve the nonlinear algebraic collocation equations for $c_i(v,Z,t)$ for any desired values of $C_i(Z,t)$ and $T(Z,t)$ in the gas phase. These solutions are used to evaluate the effectiveness factors (eqs A21 and A22, Appendix) using appropriate Gauss−Legendre quadratures.[20,21] The pressure at axial location Z and time t is computed from a fluid-mechanics-based equation (eq A4b) by the Euler technique.[20,21]

Results and Discussion

A Fortran 90 program was written to solve the equations for different idealized disturbances. The CPU time required for solving a typical dynamic simulation is 2 h on a Pentium 4 computer (1.7 GHz). The code was tested by starting from one steady state, SS1 (generated using an SS code,[6] as given in Table 1), providing a step change (at $t = 0$) in one of the operating variables, and solving until the final SS is attained. The results obtained at large values of t from the dynamic code, matched the final SS profiles generated directly.[6] The model is then used to solve two sample multiobjective optimization problems under dynamic optimal control.

Dynamic Simulation. The first problem studied involves a step increase of 100 K in the feed temperature. Nonlinear effects of the model are exhibited under such large disturbances. The axial profiles of several important variables are shown in Figure 3a−h, both at the initial and the final steady states, as well as their variations with time (in terms of deviations from the initial SS). The final SS values of the temperature (Figure 3a), are observed to be higher than the initial SS values. There is an undesirable increase (Figure 3c,d) in the outer wall temperature, $T_{w,o}$ (even small increases in $T_{w,o}$ beyond 1200 K lead to a significant reduction in the life of the reformer tubes). Higher process-gas temperatures, however, lead to higher conversions of methane (Figure 3e,f) and higher productions of CO (Figure 3g,h) and steam.[2] The mole fraction of CO_2 increases from its initial SS value in the early part of the reformer, but falls beyond some axial location. This is because of the inhibiting effect of the exothermic reaction (eq 2) at higher process-gas temperatures. Plots of both the conversion of methane and the mole fraction of CO_2 are not shown here, but can be supplied on request.

The second dynamic simulation studied here involves a step decrease of 30 kmol/h in the inlet flow rate of methane in the natural gas feed (the corresponding flow rates of the accompanying CO_2 and N_2 are also de-

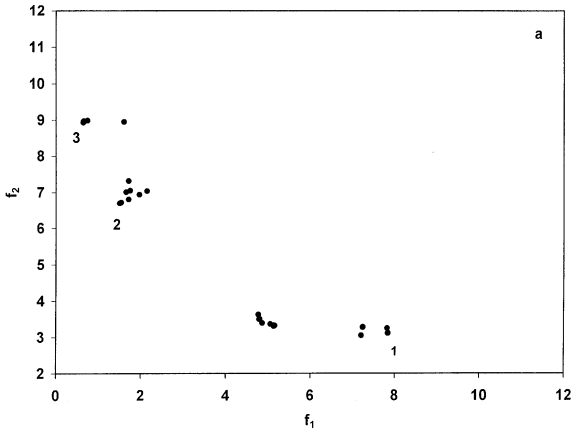
a
f_2
f_1
1
2
3

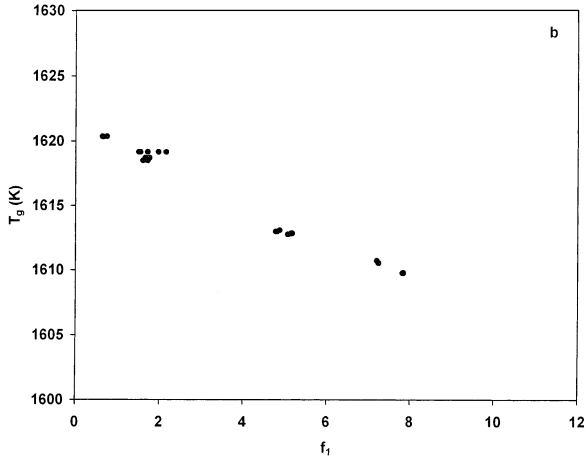
b
T_g (K)
f_1

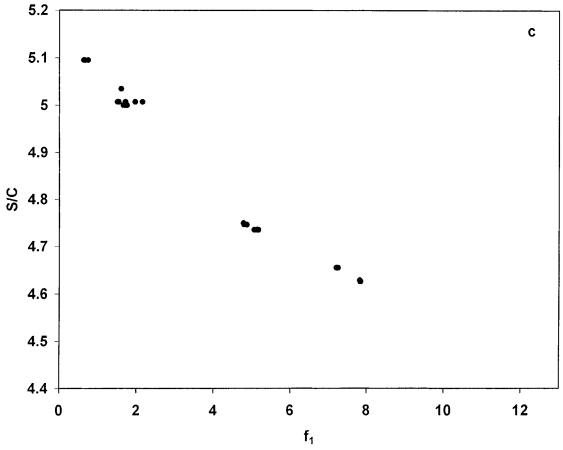
c
S/C
f_1

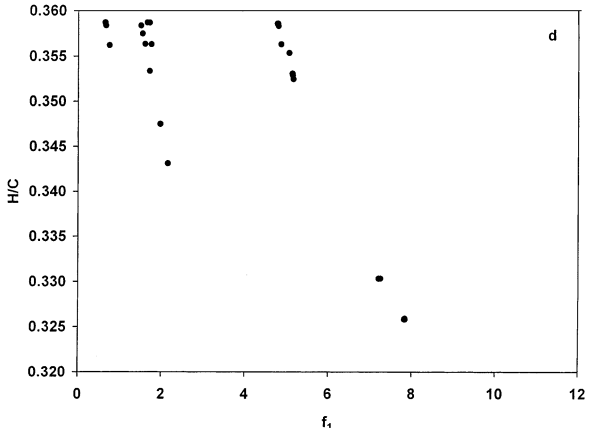
d
H/C
f_1

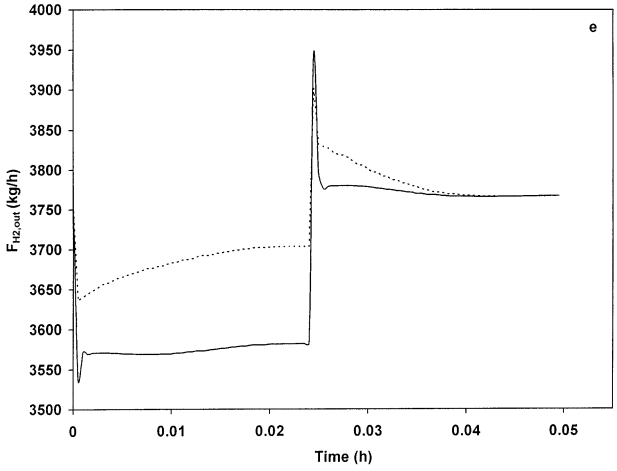
e
$F_{H2,out}$ (kg/h)
Time (h)

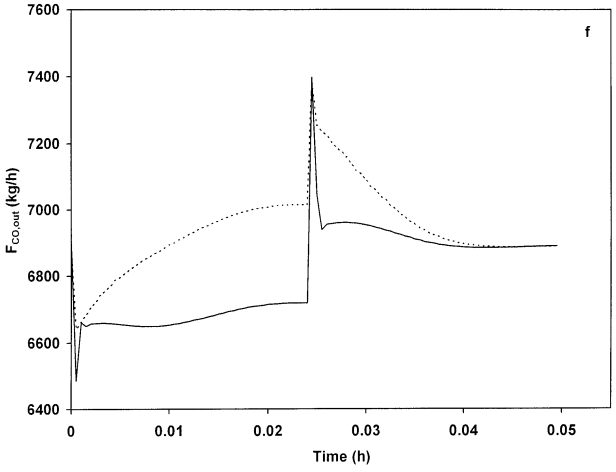
f
$F_{CO,out}$ (kg/h)
Time (h)

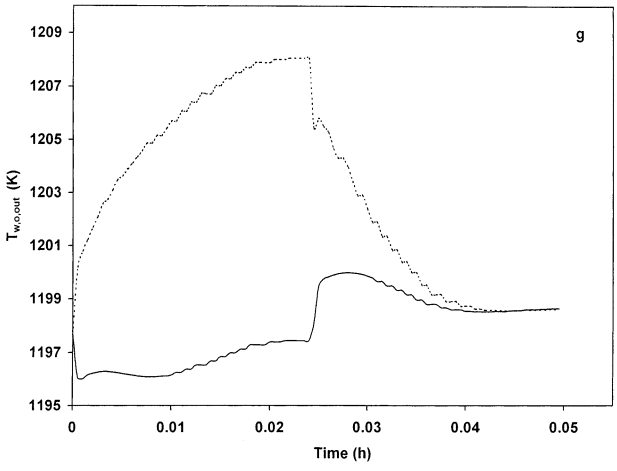
g
$T_{w,o,out}$ (K)
Time (h)

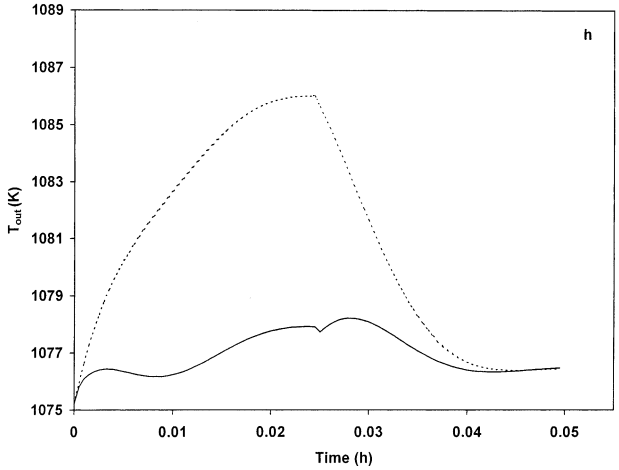
h
T_{out} (K)
Time (h)

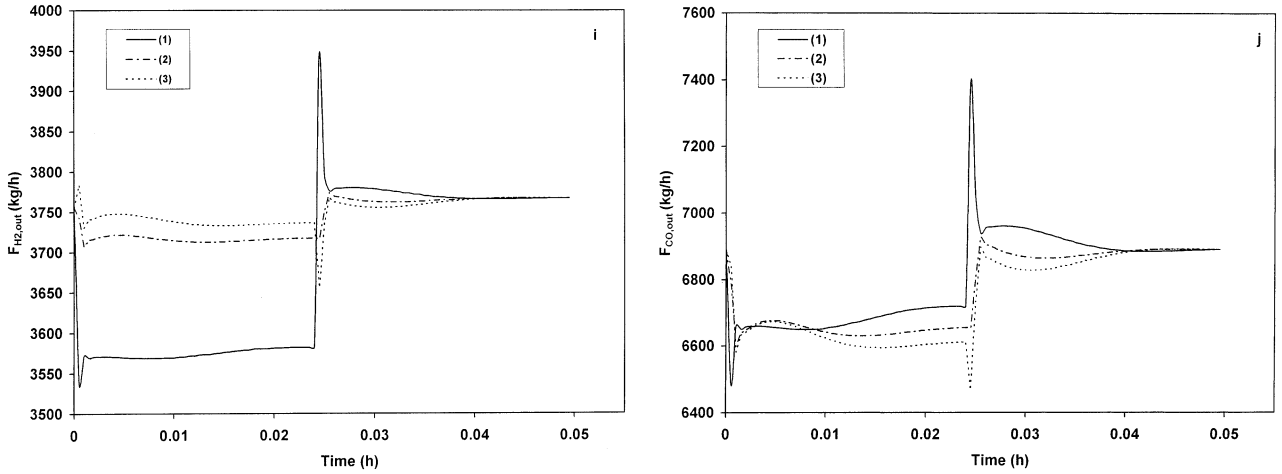

Figure 6. Pareto set, decision variables, and dynamic variations of some variables at the outlet for the multiobjective optimization problem 1 (solid line, with optimal control action; broken line, without optimal control action). Chromosome numbers 1, 2, and 3 indicated in plots i and j.

creased), while the flow rates of recycle steam and hydrogen are maintained at their original values. The superficial velocity of the process gas at the feed end decreases (from 3.24 to 3.21 m/s) immediately upon the introduction of this step disturbance, and a wave front (with a lower superficial gas velocity upstream and a higher value downstream) travels through the reformer. Because of viscous effects, this front does not actually remain sharp, so one should really solve the equations of motion (eq A4b should be replaced by the highly nonlinear PDEs of fluid mechanics) simultaneously with the reaction equations. This would make the dynamic model almost intractable. Three simpler, though empirical, approaches were explored to model this phenomenon, while still using eq A4b and keeping the CPU time reasonable. In the first approach (approach 1), we use the lower mass velocity $G_{new,in}$, at all locations and times. In approach 2, the original (higher) mass velocity is used throughout, even after the disturbance. In approach 3, which is slightly more realistic, we assume that the wave front is sharp and is traveling through the reformer tube at a constant velocity of u_{new} (= $G_{new,in}/\rho_{in}$ = 3.21 m/s). The value of t^* (= Z/u_{new}) is computed at each finite-difference grid point. This is the time at which the wave front passes the particular grid point. The new mass velocity is used at any grid point if $t \geq t^*$; otherwise, the original mass velocity is used. Figure 4a−c shows the results. These results do not differ much even at t = 3.6 s, and in fact, all three approaches give identical results (not shown) for higher values of t. Hence, one can use any one of these three approaches. Figure 4a shows some oscillations in the flow rates of H_2 at low values of t. Such behavior is characteristic of the numerical solution of problems with sharp moving fronts and can be minimized by using moving finite-element techniques, as for the far simpler "color" equation.[20,21] Figure 4d−g shows the profiles of several variables at different times.

Because of the decrease in the inlet feed rate of natural gas, the concentration of methane in the process gas decreases. This reduces the extent of the endothermic reactions (referred to as the concentration effect) and reduces the flow rates of both H_2 and CO (and steam; see Figure 4f,g). However, the higher temperatures of the process gas tend to increase the conversion to hydrogen and carbon monoxide by the endothermic reactions. This can be referred to as the temperature effect. Figure 4f and g indicates that the latter effect dominates. The complex interplay of several opposing physical phenomena is exhibited here quite well. Again, there is an increase in the outer wall temperature.

In the third dynamic simulation problem studied, a step decrease of 200 K is introduced in the furnace gas temperature. Such a disturbance can arise in industry through burner failure or a change in the feed rate of the fuel. No changes in the mass velocity are involved. Because less heat is transferred from the furnace after the disturbance, the process-gas temperature, as well as $T_{w,o}$, decreases with time to new SS values (Figure 5a,b). This leads to a simultaneous reduction in the production of H_2 and CO (and thus also steam; see Figure 5c,d). Obviously, the negative effect of such a failure on the production of desired chemicals needs to be compensated by appropriate control action, e.g., an increase in the feed temperature.

Optimization. We now study two sample optimization problems (referred to as problems 1 and 2) to illustrate the use of our dynamic model. A step pulse ($0 \leq t \leq t_T$, t_T = 0.0245 h) of −20 kmol/h in the inlet flow rate of methane is taken as the disturbance

$$F_{CH_4,in} = F_{CH_4,in,SS} \ (= 593.564 \text{ kmol/h, SS1}), \qquad t \leq 0 \text{ or } t \geq t_T$$

$$F_{CH_4,in} = F_{CH_4,in,SS} - 20 \text{ kmol/h}, \quad 0 \leq t \leq t_T \qquad (9)$$

There is a corresponding reduction in the flows of CO_2 and N_2 (in the natural gas) as well. If the input flow rates of (recycle) hydrogen and steam remained unchanged, there would be a decrease in the inlet concentration of methane. Such a decrease would lead to a decrease in the outlet conversions associated with the reforming reactions and to a decrease in the heat consumed by these endothermic reactions. If, in addition, the supply of heat from the furnace is unchanged, this would lead to an increase in the temperature, $T_{w,o}$, of the outer wall of the reformer tube. Indeed, Kvamsdal et al.[13] have shown that a decrease in the flow rate of methane could lead to thermal runaways in the reformer. This can reduce the life of the reformer tubes or cause their rupture. To counter the ill effects of this disturbance, we use the following general control action (pulse over $0 \leq t \leq t_T$)

$$T_g = T_{g,SS}\ (= 1625\ \text{K}^6), \quad t \le 0,\ t \ge t_T \tag{10a}$$

$$T_g = T_{g,SS} - \Delta T_g, \quad 0 \le t \le t_T \tag{10b}$$

$$S/C = (S/C)_{SS}\ (= 4.8^6), \quad t \le 0,\ t \ge t_T \tag{10c}$$

$$S/C = (S/C)_{SS} + \Delta(S/C), \quad 0 \le t \le t_T \tag{10d}$$

$$H/C = (H/C)_{SS}\ (= 0.34^6), \quad t \le 0,\ t \ge t_T \tag{10e}$$

$$H/C = (H/C)_{SS} + \Delta(H/C), \quad 0 \le t \le t_T \tag{10f}$$

The decision variables are, thus, ΔT_g, $\Delta(S/C)$, and $\Delta(H/C)$.

Two objective functions are minimized simultaneously. They are the total (cumulative over t) deviations[22] of the production of (a) hydrogen and (b) steam, from their SS1 values, integrated over an appropriately long time span, $0 \le t \le t_f$ ($t_f = 0.05$ h), so that their rates of production reattain their initial steady-state values. The flow rate of steam is related to that of CO, and we can minimize the cumulative deviation of the production of CO.[6] The final optimization problem (referred to as problem 1) is written mathematically (along with the constraints and bounds) as

Problem 1

$$\min f_1[\Delta T_g,\Delta(S/C),\Delta(H/C)] \equiv \int_0^{t_f}[F_{H_2,SS,out} - F_{H_2,out}(t)]\,dt \tag{11a}$$

$$\min f_2[\Delta T_g,\Delta(S/C),\Delta(H/C)] \equiv \int_0^{t_f}[F_{CO,SS,out} - F_{CO,out}(t)]\,dt \tag{11b}$$

subject to (s.t.) the constraint

$$T_{w,o} \le 1200\ \text{K} \tag{11c}$$

and the bounds

$$-25 \le \Delta T_g \le 5 \tag{11d}$$

$$-0.4 \le \Delta(S/C) \le 0.3 \tag{11e}$$

$$-0.02 \le \Delta(H/C) \le 0.02 \tag{11f}$$

In eqs 11, $F_{H_2,out}(t)$ and $F_{CO,out}(t)$ are the mass flow rates of H_2 and CO, respectively, in the syngas exiting the reformer. It can be noted that we do not use the squares of the integrands in eqs 11a and b, because any short-term increases in the flow rates above the steady-state values need not be penalized because they are beneficial. The constraint on $T_{w,o}$ is that used by Rajesh et al.[6] In these equations, the bounds on $\Delta(S/C)$ and $\Delta(H/C)$ are taken to be about 5% of the SS values and are of the same order as the deviation in the methane flow rate.

The following penalty[23] is added to both objective functions

$$P \equiv 10^4[(T_{w,o} - 1200) + \text{abs}(T_{w,o} - 1200)] \tag{12}$$

to take care of the constraint on $T_{w,o}$. (Alternatives exist.[23]) The multiplier (10^4) was sufficiently large, and the results were found to be insensitive to an increase in its value.

The second multiobjective optimization problem (problem 2) involves a pulse decrease in the feed temperature

$$T_{in} = T_{in,SS}\ (= 841.7\ \text{K}^6), \quad t \le 0,\ t \ge t_T$$

$$T_{in} = T_{in,SS} - 50\ \text{K}, \quad 0 \le t \le t_T \tag{13}$$

with t_T taken as 0.023 h (slightly different than for problem 1). Because of the decrease in the inlet feed temperature, the outlet temperature of the syngas and the conversion of methane decrease. This results in a decrease in the production of both hydrogen and steam. The effects of this disturbance are negated once again using step changes in the furnace gas temperature, T_g; the steam-to-methane ratio, S/C; and the hydrogen-to-methane ratio, H/C, as follows

$$T_g = T_{g,SS}\ (= 1625\ \text{K}^6), \quad t \le t_1 \text{ or } t \ge t_2 \tag{14a}$$

$$T_g = T_{g,SS} + \Delta T_g, \quad t_1 \le t \le t_2 \tag{14b}$$

$$S/C = (S/C)_{SS}\ (= 4.8^6), \quad t \le t_1 \text{ or } t \ge t_2 \tag{14c}$$

$$S/C = (S/C)_{SS} + \Delta(S/C), \quad t_1 \le t \le t_2 \tag{14d}$$

$$H/C = (H/C)_{SS}\ (= 0.34^6), \quad t \le t_1 \text{ or } t \ge t_2 \tag{14e}$$

$$H/C = (H/C)_{SS} + \Delta(H/C), \quad t_1 \le t \le t_2 \tag{14f}$$

t_1 and t_2 are additional decision variables used to make the problem general. An increase in the temperature of the furnace gas increases the heat content of the reformer gases and helps compensate for the effect of the decrease in the inlet feed temperature. Higher steam-to-methane ratios help to increase the hydrogen production, while higher hydrogen-to-methane ratios increase the carbon monoxide (and, therefore, also the steam) production. Problem 2 can, thus, be written as

Problem 2

$$\min f_1[\Delta T_g,\Delta(S/C),\Delta(H/C),t_1,t_2] \equiv \int_0^{t_f}[F_{H_2,SS,out} - F_{H_2,out}(t)]\,dt \tag{15a}$$

$$\min f_2[\Delta T_g,\Delta(S/C),\Delta(H/C),t_1,t_2] \equiv \int_0^{t_f}[F_{CO,SS,out} - F_{CO,out}(t)]\,dt \tag{15b}$$

s.t.

$$T_{w,o} \le 1200\ \text{K} \tag{15c}$$

$$-15 \le \Delta T_g \le 25\ \text{K} \tag{15d}$$

$$-0.4 \le \Delta(S/C) \le 0.3 \tag{15e}$$

$$-0.03 \le \Delta(H/C) \le 0.03 \tag{15f}$$

$$0 \le t_1 \le 0.023\ \text{h} \tag{15g}$$

$$0.023 \le t_2 \le 0.058\ \text{h} \tag{15h}$$

with $t_f = 0.058$ h. The lower bound on ΔT_g is relatively unimportant because, intuitively, it is expected that ΔT_g will be positive. The upper bound on ΔT_g was determined on the basis of the normal operating conditions possible in industrial reformers. The ranges of $\Delta(S/C)$

Table 2. GA Parameters Used for Optimization

parameter	problem 1	problem 2
total chromosome length (N_{chr})	22	20
population size (N_p)	70	50
number of generations (N_{ga})	9	18
crossover probability (p_c)	0.95	0.95
mutation probability (p_m)	0.01	0.05
random seed number	0.888 76	0.888 76

and $\Delta(H/C)$ were determined on the basis of the magnitude of the disturbance. The lower bound on t_1 is the time at which the disturbance is introduced ($t = 0$), while the upper bound (and the lower bound on t_2) is set at a conservatively high value of t_T, the time at which the input disturbance ceases (higher values of t_1 are nonoptimal). The upper bound on t_2 is the time corresponding to the final steady state, t_f. The value of t_f is selected on the basis of experience with simulation runs.

The recently developed robust and efficient technique called the elitist nondominated sorting genetic algorithm (NSGA-II)[23,24] is used to solve these problems. The parameters associated[23−25] with NSGA-II for problems 1 and 2 are given in Table 2. The CPU times required to solve problems 1 (9 generations) and 2 (18 generations) on a Silicon Graphics server (SGI origin 270, 400 MHz) are 110 and 144 h, respectively. The highly computationally intensive nature of these problems puts constraints on the number of runs (or the size of populations or the number of generations), and we have to be content with the reasonable Pareto solutions obtained. Because the main focus in this paper was not optimization, we did not explore other techniques (e.g., using parallel computing platforms or developing empirical and faster model equations) to improve the solutions. Several checks were made on our code, as discussed by Kasat et al.,[26] to ensure that the solutions obtained were correct. In addition, we used the ϵ-constraint technique[27] (in which one objective function is taken as a constant, ϵ, to form an additional constraint and the resulting single-objective-function optimization problem is solved using a different code) and found that the solutions matched those obtained using NSGA-II, confirming that we did, indeed, attain optimal solutions.

The results for problem 1 are shown in Figure 6. If we go from any one point (say, 1) to another (say, 2) in Figure 6a, we find that f_1 improves (decreases) whereas f_2 worsens (increases). This plot, therefore, represents a Pareto set.[23−25] Clearly, the control action taken to negate the effect of this disturbance is unable to increase the rates of production of both hydrogen and steam. A decision maker would have to decide on the preferred solution (operating point) from among these several, equally good, Pareto points. Figure 6b−d shows the corresponding decision variables (actual values). High values of T_g and the S/C ratio are associated with lower f_1 values (larger hydrogen production) and higher f_2 values (lower CO or steam production) under optimal conditions. The optimal values of H/C do not appear to exhibit any definite trend, and we believe that there is some scatter in these data. Such scatter in one or more decision variables seems to be the norm rather than an exception for most real-life problems[25] and to reflect the relative insensitivity of the objective functions to variations in these decision variables. As mentioned before, the results could be improved but at the cost of excessive computational effort. A study of several members of the initial (nonoptimal) solutions reveals that chromosomes having high values of T_g and relatively low values of S/C violate the constraint on the outer wall temperature, $T_{w,o}$, and are "killed" over the generations. Table 3 reports the values of the decision variables for three different chromosomes, 1−3 (in Figure 6a), in the Pareto set.

Table 3. Decision Variables (in Nondeviation Form) and Objective Functions for Three Chromosomes in Figure 6a

decision variable	chromosome		
	1	2	3
T_g	1609.8	1619.2	1620.4
S/C	4.63	5.01	5.09
H/C	0.326	0.358	0.359
f_1	3.12	1.50	0.645
f_2	7.84	6.69	8.92

The variation of several important variables over time, both in the absence (broken curves) and in the presence (continuous curves) of optimal control action for chromosome 1, are shown in Figure 6e−h. It is observed that the outer tube-wall temperature at the exit (the highest value in the reformer) under optimal conditions hovers around its bound of 1200 K (see Figure 6g). If control action were not used, the tube-wall temperature would violate this constraint. This simultaneously leads to the gas temperature at the exit of the reformer lying near its steady-state value of 1076 K. The lower process-gas temperatures in the presence of optimal control lead to lower conversions of methane and lower productions of both hydrogen and carbon monoxide/steam. Figure 6i and j shows the variations of the exit flow rates of both hydrogen and carbon monoxide for chromosomes 1−3. Chromosomes having high values of S/C (e.g., chromosome 3) are associated with a lower cumulative deviation in the flow rate of hydrogen but a higher deviation in the flow rate of carbon monoxide.

Figure 7a shows the Pareto set at the 18th generation for problem 2. It can be noted that negative values (high total production of hydrogen under dynamic control) of f_1 are obtained here. This, of course, occurs with a worsening of f_2. Figure 7b−f shows the corresponding decision variables. It is observed that the furnace gas temperature, T_g, remains at slightly higher values (than the SS value) for all of the Pareto points. In contrast, S/C and t_2 decrease as the optimal value of f_1 increases. The optimal values of t_1 remain near their lower bounds. Figure 7g−j shows the variations of some important variables over time for chromosome 2 of the Pareto set. The high value of S/C used for this chromosome increases the production of hydrogen (to even better values than in the absence of the disturbance; see Figure 7i) and reduces the production of carbon monoxide and steam. Figure 7k and l shows the variations of the exit flow rates of both hydrogen and carbon monoxide with time for chromosomes 1−3 in Figure 7a. It can be observed from these diagrams that chromosomes having higher S/C values have lower deviations in the exit flow rate of hydrogen and higher deviations in the exit flow rate of carbon monoxide. High values of T_g improve both objective functions. Table 4 provides values of the decision variables for the three different chromosomes, 1−3, shown in Figure 7a.

Conclusions

A dynamic model for the first reactor, the reformer, in a steam reformer plant is presented. The effects of a

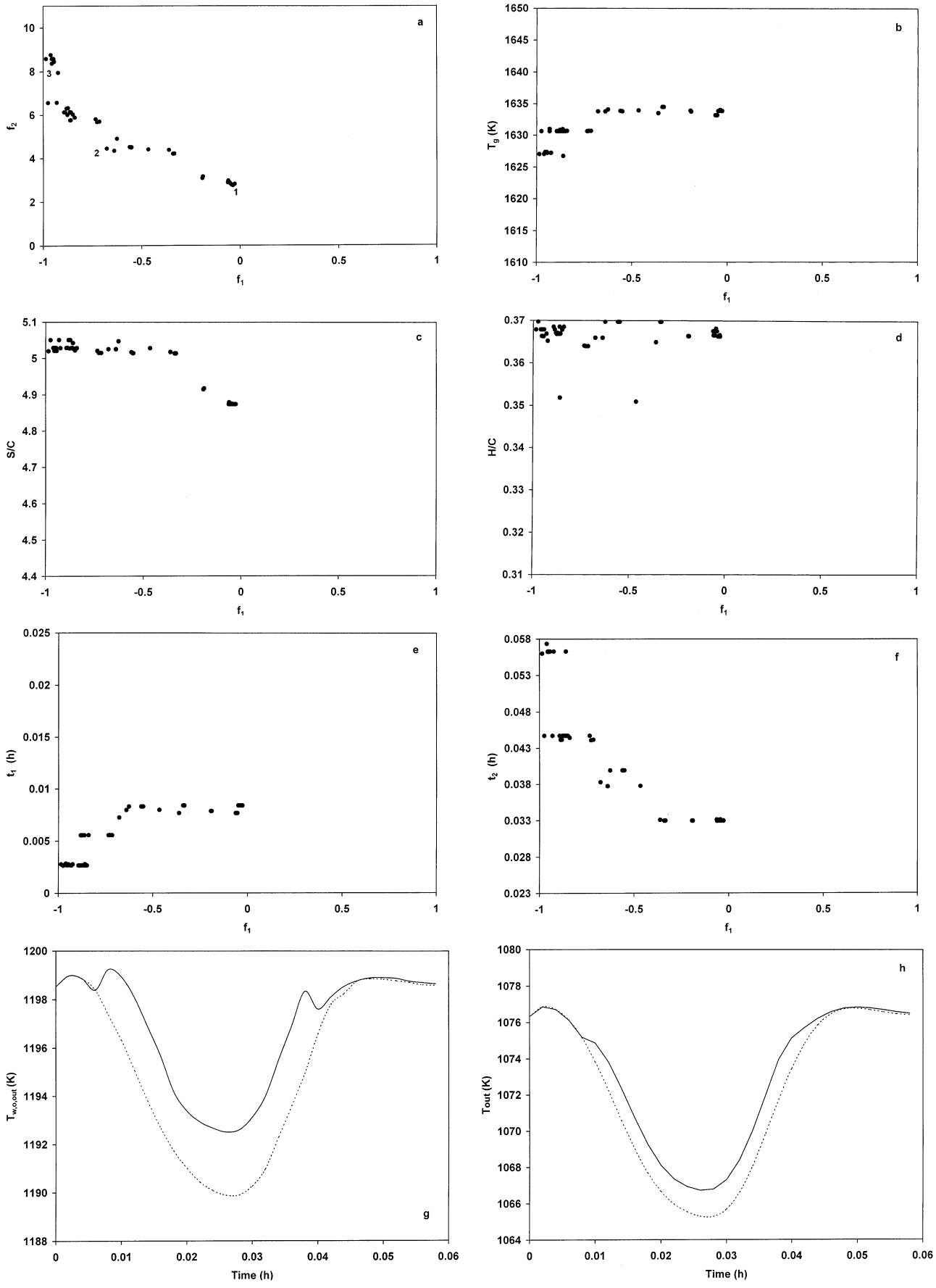
a
f_2
f_1
1
2
3
b
T_g (K)
f_1
c
S/C
f_1
d
H/C
f_1
e
t_1 (h)
f_1
f
t_2 (h)
f_1
g
$T_{w,o,out}$ (K)
Time (h)
h
Tout (K)
Time (h)

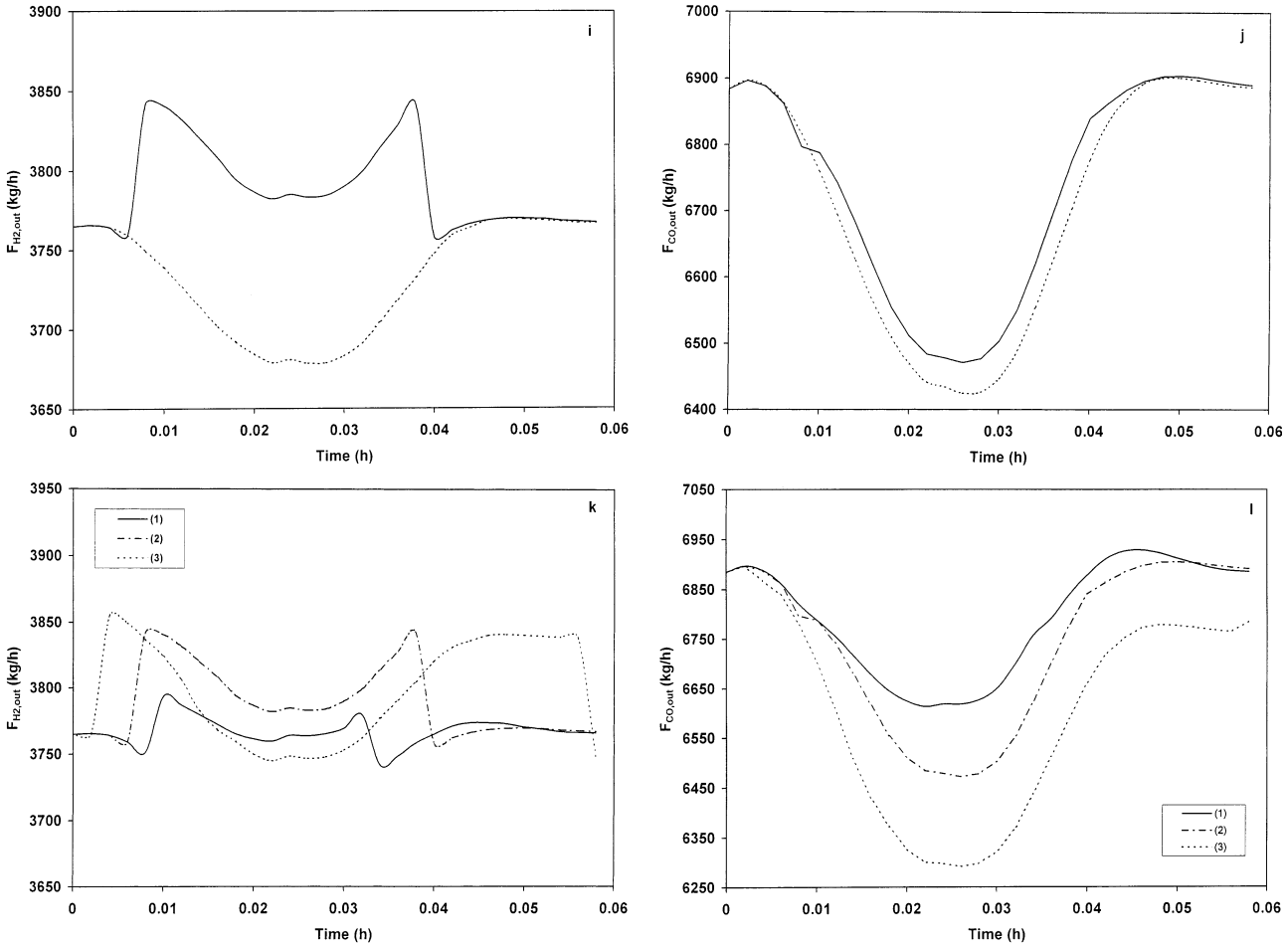

Figure 7. Pareto set, decision variables, and dynamic variations of some variables at the outlet, for the multiobjective optimization problem 2 (solid line, with optimal control action; broken line, without optimal control action). Chromosome numbers 1, 2, and 3 indicated in plots k and l.

Table 4. Decision Variables (in Nondeviation Form) and Objective Functions for Three Chromosomes in Figure 7a

decision variable	chromosome		
	1	2	3
T_g	1633.8	1633.8	1627.1
S/C	4.87	5.03	5.02
H/C	0.367	0.366	0.368
t_1	0.0084	0.00726	0.0028
t_2	0.0331	0.0383	0.056
f_1	−0.0443	−0.679	−0.986
f_2	2.79	4.44	8.59

few idealized disturbances are studied. The model is then used to study two sample multiobjective optimization problems for this reactor, and Pareto-optimal solutions are obtained. An extensive file of similar optimal control actions under a variety of disturbances can be generated for later use.

Acknowledgment

Partial financial support from the Department of Science and Technology, Government of India, New Delhi, India [through grant III-5(13)/2001-ET] is gratefully acknowledged.

Nomenclature

a = fractional length of the half-catalyst slab in which the concentration varies
A_c = inside cross-sectional area of the reformer tube, m^2
A_f = surface area of the flame produced by a single burner, m^2
A_p = cross-sectional area of the catalyst slab, m^2
A_{ref} = surface area of the refractor, m^2
$A_{t,i}$ = total internal surface area of reformer tubes, m^2
c_i = concentration of species i in the catalyst slab, kmol m^{-3}
C_i = concentration of species i in the gas phase, kmol m^{-3}
$C_{p,g}$ = specific heat of the process gas, kJ $kmol^{-1}$ K^{-1}
$C_{p,s}$ = specific heat of the solid (catalyst), kJ $kmol^{-1}$ K^{-1}
$C_{p,t}$ = specific heat of the bed, kJ $kmol^{-1}$ K^{-1}
C_t = molar concentration of the gas mixture (= P/RT), kmol m^{-3}
d_i, d_o = inner and outer diameters, respectively, of the reformer tube, m
D_i^e = effective diffusivity of species i in the catalyst at axial location Z and time t, m^2 h^{-1}
D_p = equivalent diameter of the catalyst pellet (Raschig ring), m
D/C = ratio of carbon dioxide to methane in feed, (kmol/h of CO_2)/[kmol/h of methane fed ($F_{CH_4,in}$)]
E = quantity defined in eq A11
f_i = objective function, i = 1, 2
F = total feed rate, kmol h^{-1}
F_{CH_4} = flow rate of methane, kg h^{-1}
F_{CO} = flow rate of CO, kg h^{-1}
F_{H_2} = flow rate of H_2, kg h^{-1}
G = mass velocity of the process gas in the reformer, kg m^{-2} h^{-1}
H/C = ratio of hydrogen to methane in feed, (kmol/h of hydrogen recycled)/[kmol/h of methane fed ($F_{CH_4,in}$)]

ΔH_i = enthalpy of the ith reaction, kJ kmol^{-1}
k_g = thermal conductivity of the process gas, kJ h^{-1} m^{-1} K^{-1}
k_w = thermal conductivity of the tube-wall material, kJ h^{-1} m^{-1} K^{-1}
k_i = rate constant of the ith (i = I−III) reaction, kmol kPa$^{0.5}$ kg$_{cat}^{-1}$ h^{-1} or kmol kPa^{-1} kg$_{cat}^{-1}$ h^{-1}
K_I, K_{II}, K_{III} = equilibrium constants of reactions I−III, respectively
K_i = equilibrium adsorption constant for species i (i = CH_4, H_2, CO, H_2O), kPa^{-1}
l = axial location in the catalyst slab, m
l_c = thickness of the wall of the Raschig ring, m
l_p = length of the Raschig ring, m
L = total length of the reactor, m
M = number of internal collocation points
N/C = ratio of carbon dioxide to methane in feed, (kmol/h of nitrogen)/[kmol/h of methane fed ($F_{CH_4,in}$)]
N_b = number of burners in the reformer furnace
N_{chr} = total chromosome length for NSGA-II
N_{ga} = number of generations for NSGA-II
N_i = flux of species i at any axial location l inside the catalyst slab, kmol m^{-2} h^{-1}
N_p = population size for NSGA-II
p_c = probability of crossover
p_m = probability of mutation
P = operating pressure at axial location Z and time t, kPa
q_{cond} = conductive heat flux based on the average surface area of the tube, kJ m^{-2} h^{-1}
q_{conv} = convective heat flux based on the inner surface area of the tube, kJ m^{-2} h^{-1}
q_{rad} = radiative heat flux based on the outer surface area of the tube, kJ m^{-2} h^{-1}
r = radial position, m
r_i = rate of the ith reaction (i = I−III) corresponding to conditions at the catalyst surface at axial location Z and time t, kmol h^{-1} kg$_{cat}^{-1}$
R = sum of feed molar ratios
R_i = rate of production of the ith component at the catalyst surface at any axial location Z and time t, kmol h^{-1} kg$_{cat}^{-1}$
$R_{i,n}$ = rate of production of the ith component at the nth collocation point inside the catalyst slab at axial location Z and time t, kmol h^{-1} kg$_{cat}^{-1}$
S/C = ratio of carbon dioxide to methane in feed, (kmol/h of steam recycled)/[kmol/h of methane fed ($F_{CH_4,in}$)]
t = time, h
T = process-gas temperature at axial location Z and time t, K
T_f = adiabatic flame temperature at any axial location in the reactor, K
T_g = temperature of the furnace gas, K
T_w = tube-wall temperature, K
U = film heat-transfer coefficient on the inside of the tube (to gas + catalyst), kJ h^{-1} m^{-2} K^{-1}
v = dimensionless distance within the catalyst slab (= l/l_c) (v = 0 at catalyst surface)
v_l = superficial velocity of gas in the reformer, m h^{-1}
y_i = mole fraction of species i in the gas phase at axial location Z and time t
$\bar{y}_{i,n}$ = mole fraction of component i at the nth collocation point inside the catalyst slab at axial location Z and time t
Z = axial location, m

Greek Symbols

ϵ_b = void fraction in the catalyst bed (outside the porous catalyst pellet)
ϵ_c = volume fraction of pores inside a catalyst pellet
η_I, η_{II},η_{III} = effectiveness factors for reactions I−III, respectively, at axial location Z and time t
η_i = effectiveness factor for component i at axial location Z and time t
μ = viscosity of the gas mixture at axial location Z and time t, kg m^{-1} h^{-1}
ξ_g = emissivity of the furnace gas
ξ_f = emissivity of the flames
ξ_t = emissivity of the tube material
ρ_b = density of the catalyst bed (solid + voids + pores), kg m^{-3}
ρ_g = density of the gas mixture, kg m^{-3}
ρ_s = density of the catalyst pellet (solid + pores), kg m^{-3}
σ = Stefan−Boltzmann constant, kJ h^{-1} m^{-2} K^{-4}
σ_{ik} = stoichiometric coefficient of the ith component participating in the kth reaction
τ = tortuosity of the catalyst pellet
ϕ_s = sphericity of the catalyst pellet

Subscripts/Superscripts

i, 1 = inner or initial
in = inlet of the reformer
o, 2 = outer
out = outlet of the reformer
SS = steady state
SS1 = initial steady state
w = wall

Appendix

Model Equations.[2,6]

$$F_{CH_4,in} = 16\frac{F}{R},$$
$$\text{where } R = [1 + (S/C) + (H/C) + (D/C) + (N/C)] \quad \text{(A1)}$$

$$F_{H_2,out} = 2C_{H_2,out}(v_{l,out}A_c) \quad \text{(A2)}$$

$$F_{CO,out} = 28C_{CO,out}(v_{l,out}A_c) \quad \text{(A3)}$$

(a) Gas Phase

$$\frac{\partial C_i}{\partial t} = \frac{1}{\epsilon_b}\left[\frac{\partial(v_l C_i)}{\partial Z} - \rho_b \eta_i R_i\right],$$
$$i = CH_4,\ H_2O,\ CO,\ CO_2,\ H_2 \quad \text{(A4a)}$$

$$\frac{\partial P}{\partial Z} = -\frac{1.75G^2(1-\epsilon_b)}{\phi_s D_p \epsilon_b^{\,3} \rho_g} \quad \text{(A4b)}$$

$$\frac{\partial T}{\partial t} = \frac{1}{C_{p,t}}\left[\frac{4U(T_{w,i} - T)}{d_i} - \rho_g C_{p,g} v_l \frac{\partial T}{\partial Z} + \rho_b \sum_{i=I}^{III}(-\Delta H_i)\eta_i r_i\right] \quad \text{(A4c)}$$

$$C_{p,t} = \rho_b C_{p,s} + [\epsilon_b + (1-\epsilon_b)\epsilon_c]\rho_g C_{p,g} \quad \text{(A4d)}$$

Initial Conditions

$$C_i(Z,t{=}0) = C_i^{SS}(Z),$$
$$0 \le Z \le L;\ i = CH_4,\ H_2O,\ CO,\ CO_2,\ H_2 \quad \text{(A4e)}$$

$$P(Z,t=0) = P^{SS}(Z), \quad 0 \le Z \le L \tag{A4f}$$

$$T(Z,t=0) = T^{SS}(Z), \quad 0 \le Z \le L \tag{A4g}$$

$$y_i = C_i/C_t, \quad i = CH_4, H_2O, CO, CO_2, H_2 \tag{A5}$$

$$y_{N_2} = 1 - (y_{CH_4} + y_{H_2O} + y_{CO} + y_{CO_2} + y_{H_2}) \tag{A6}$$

$$R_i = \sum_{k=I}^{III} \sigma_{ik} r_k, \quad i = CH_4, H_2O, CO, CO_2, H_2 \tag{A7}$$

$$r_I = \frac{k_I}{E^2 y_{H_2}{}^{2.5}\sqrt{P}}\left(y_{CH_4} y_{H_2O} - \frac{P^2 y_{H_2}{}^3 y_{CO}}{K_I}\right) \tag{A8}$$

$$r_{II} = \frac{k_{II} P}{E^2 y_{H_2}}\left(y_{CO} y_{H_2O} - \frac{y_{H_2} y_{CO_2}}{K_{III}}\right) \tag{A9}$$

$$r_{III} = \frac{k_{III}}{E^2 y_{H_2}{}^{3.5}\sqrt{P}}\left(y_{CH_4} y_{H_2O}{}^2 - \frac{P^2 y_{H_2}{}^4 y_{CO_2}}{K_I K_{II}}\right) \tag{A10}$$

$$E = \left[1 + P(K_{CO} y_{CO} + K_{CH_4} y_{CH_4} + K_{H_2} y_{H_2}) + K_{H_2O}\frac{y_{H_2O}}{y_{H_2}}\right] \tag{A11}$$

The inner tube wall temperature, $T_{w,i}$, is obtained by equating the heat fluxes due to (i) radiative transfer from the furnace gases to the exterior surface of the tubes

$$q_{rad} = \sigma\frac{(A_{t,o} + A_{ref})\xi_g \xi_t}{(A_{t,o} + A_{ref})\xi_g + A_{t,o}(1 - \xi_g)\xi_t}(T_g{}^4 - T_{w,o}{}^4) + \sigma\frac{N_b A_f \xi_f \xi_t (1 - \xi_g)}{A_{t,o}} T_f{}^4 \tag{A12}$$

(ii) conductive transfer through the tube material

$$q_{cond} = \frac{2k_w(T_{w,o} - T_{w,i})}{\ln(d_o/d_i)} \tag{A13}$$

and (iii) convective transfer to the gas mixture and catalyst bed from the inner surface of the tubes

$$q_{conv} = U(T_{w,i} - T) \tag{A14}$$

$$U = 0.4\frac{k_g}{D_p}\left[2.58\left(\frac{D_p G}{\mu}\right)^{1/3}\left(\frac{C_{p,g}\mu}{k_g}\right)^{1/3} + 0.094\left(\frac{D_p G}{\mu}\right)^{0.8}\left(\frac{C_{p,g}\mu}{k_g}\right)^{0.4}\right] \tag{A15}$$

(b) Solid (Catalyst) Phase. The intraparticle mole fraction, $\bar{y}_{i,n}(v)$, of species i at the nth orthogonal collocation point for a catalyst slab at axial location Z and time t is obtained by solving the coupled set of $5M$ equations ($n = 1$ is the first collocation point at $v = 0$; $n = M + 2$ is the last collocation point at $v = 0.2$; $n = 2, 3, ..., M + 1$ are the internal collocation points in $0 \le v \le 0.2$): $3M$ algebraic and $2M$ differential equations (which are transformed into algebraic equations by the method of orthogonal collocation on finite elements)

$$\frac{d^2\bar{y}_{CH_4,n}}{dv^2} = a^2 l_c{}^2\left[\frac{\rho_s(r_I + r_{II} + r_{III})_b}{(P/RT)D^e_{CH_4}}\right]\frac{R_{CH_4,n}}{R_{H_2O,I}}, \quad n = 2, 3, ..., M + 1 \tag{A16}$$

$$\frac{d^2\bar{y}_{H_2O,n}}{dv^2} = a^2 l_c{}^2\left[\frac{\rho_s(r_I + r_{II} + 2r_{III})_b}{(P/RT)D^e_{H_2O}}\right]\frac{R_{H_2O,n}}{R_{H_2O,I}}, \quad n = 2, 3, ..., M + 1 \tag{A17}$$

$$\bar{y}_{CO,n} = y_{CO} - \frac{1}{D^e_{CO}}[2D^e_{CH_4}(\bar{y}_{CH_4,n} - y_{CH_4}) - D^e_{H_2O}(\bar{y}_{H_2O,n} - y_{H_2O})], \quad n = 2, 3, ..., M + 1 \tag{A18}$$

$$\bar{y}_{CO_2,n} = y_{CO_2} + \frac{1}{D^e_{CO_2}}[D^e_{CH_4}(\bar{y}_{CH_4,n} - y_{CH_4}) - D^e_{H_2O}(\bar{y}_{H_2O,n} - y_{H_2O})], \quad n = 2, 3, ..., M + 1 \tag{A19}$$

$$\bar{y}_{H_2,n} = y_{H_2} - \frac{1}{D^e_{H_2}}[2D^e_{CH_4}(\bar{y}_{CH_4,n} - y_{CH_4}) + D^e_{H_2O}(\bar{y}_{H_2O,n} - y_{H_2O})], \quad n = 2, 3, ..., M + 1 \tag{A20}$$

(where the rates, R_i, are given in eqs A7−A11)

Boundary Conditions

(at Axial Location Z and Time t)

$$\bar{y}_{i,1} = y_i(Z,t), \quad i = CH_4, H_2O, CO, CO_2, H_2$$

$$\frac{d\bar{y}_{i,M+2}}{dv} = 0, \quad i = CH_4, H_2O, CO, CO_2, H_2$$

$$\eta_k = \frac{\int_{v=0}^{v=a} r_k(\bar{y}_i,T,P)\,dv}{r_k(y_i,T,P)l_c}, \quad k = I, II, III \tag{A21}$$

Effectiveness factors for the components are evaluated from those for the reactions[2] through the equation

$$\eta_i = \frac{\sum_{k=I}^{III}\sigma_{ik}\eta_k r_k}{\sum_{k=I}^{III}\sigma_{ik} r_k}, \quad i = CH_4, H_2O, CO, CO_2, H_2 \tag{A22}$$

Literature Cited

(1) Armor, J. N. The Multiple Roles for Catalysis in the Production of H_2. *Appl. Catal. A* **1999**, *176*, 159.

(2) Elnashaie, S. S. E. H.; Elshishini, S. S. *Modeling, Simulation and Optimization of Industrial Catalytic Fixed Bed Reactors*; Gordon and Breach: Amsterdam, The Netherlands, 1993.

(3) Xu, J.; Froment, G. F. Methane Steam Reforming, Methanation and Water−Gas Shift: I. Intrinsic Kinetics. *AIChE J.* **1989**, *35*, 88.

(4) Xu, J.; Froment, G. F. Methane Steam Reforming: II. Diffusional Limitations and Reactor Simulation. *AIChE J.* **1989**, *35*, 97.

(5) Singh, C. P. P.; Saraf, D. N. Simulation of Side Fired Steam−Hydrocarbon Reformers. *Ind. Eng. Chem. Process Des. Dev.* **1979**, *18*, 1.

(6) Rajesh, J. K.; Gupta, S. K.; Rangaiah, G. P.; Ray, A. K. Multiobjective Optimization of Steam Reformer Performance Using Genetic Algorithm. *Ind. Eng. Chem. Res.* **2000**, *39*, 706.

(7) Elnashaie, S. S. E. H.; Elshishini, S. S. *Dynamic Modelling, Bifurcation and Chaotic Behaviour of Gas−Solid Catalytic Reactors*; Gordon and Breach: Amsterdam, The Netherlands, 1996.

(8) Alatiqi, I. M. Online Quality Control Methods for Steam−Gas Reformers. *Int. J. Hydrogen Energy* **1990**, *15*, 179.

(9) Alatiqi, I. M.; Meziou, A. M. Dynamic Simulation and Adaptive Control of an Industrial Steam Reformer. *Comput. Chem. Eng.* **1991**, *15*, 147.

(10) Meziou, A. M.; Deshpande P. B.; Alatiqi, I. M. Dynamic Matrix Control of an Industrial Steam Gas Reformer. *Int. J. Hydrogen Energy* **1995**, *20*, 187.

(11) Alatiqi, I. M.; Meziou, A. M.; Gasmelseed, G. A. Modeling, Simulation and Sensitivity Analysis of Steam−Methane Reformers. *Int. J. Hydrogen Energy* **1989**, *14*, 241.

(12) Meziou, A. M.; Alatiqi, I. M. Identification and Control of an Industrial Steam-Reforming Plant. *Can. J. Chem. Eng.* **1994**, *72*, 321.

(13) Kvamsdal, H. M.; Svendsen, H. F.; Hertzberg, T.; Olsvik O. Dynamic Simulation and Optimization of a Catalytic Steam Reformer. *Chem. Eng. Sci.* **1999**, *54*, 2697.

(14) Serbezov, A.; Sotirchos, S. V. Particle-Bed Model for Multicomponent Adsorption-based Separations: Applications to Pressure Swing Adsorption. *Chem. Eng. Sci.* **1999**, *54*, 5647.

(15) Froment, G. F.; Bischoff, K. B. *Chemical Reactor Analysis and Design*, 2nd ed.; Wiley: New York, 1990.

(16) Deken, J. C. D.; Devos, E. F.; Froment, G. F. Steam Reforming of Natural Gas: Intrinsic Kinetics, Diffusional Influences, and Reactor Design. *ACS Symp. Ser.* **1982**, *196*, 181.

(17) Villadsen, J.; Michelsen, M. L. *Solution of Differential Equation Models by Polynomial Approximation*; Prentice Hall: Englewood Cliffs, NJ, 1978.

(18) Seader, J. D.; Henley, E. J. *Separation Process Principles*; Wiley: New York, 1997.

(19) Plehiers, P. M.; Froment, G. F. Coupled Simulation of Heat Transfer and Reaction in a Steam Reforming Furnace. *Chem. Eng. Technol.* **1989**, *12*, 20.

(20) Finlayson, B. A. *Nonlinear Analysis in Chemical Engineering;* McGraw-Hill: New York, 1980.

(21) Gupta, S. K. *Numerical Methods for Engineers*; Wiley Eastern/New Age International: New Delhi, India, 1995.

(22) Ray, W. H.; Szekely, J. *Process Optimization;* Wiley: New York, 1973.

(23) Deb, K. *Multi-Objective Optimization Using Evolutionary Algorithms*. Wiley: Chichester, U.K., 2001.

(24) Deb, K.; Pratap, A.; Agarwal, S.; Meyarivan, T. A Fast and Elitist Multiobjective Genetic Algorithm: NSGA-II. *IEEE Trans. Evol. Comput.* **2002**, *182*, 6.

(25) Bhaskar, V.; Gupta, S. K.; Ray, A. K. Applications of Multiobjective Optimization in Chemical Engineering. *Rev. Chem. Eng.* **2000**, *16*, 1.

(26) Kasat, R. B.; Kunzru, D.; Saraf, D. N.; Gupta, S. K. Multiobjective Optimization of Industrial FCC Unit Using Elitist Nondominated Sorting Genetic Algorithm. *Ind. Eng. Chem. Res.* **2002**, *4765*, 41.

(27) Chankong, V.; Haimes, Y. Y. *Multiobjective Decision Making−Theory and Methodology*; Elsevier: New York, 1983.

Received for review December 3, 2002
Revised manuscript received April 15, 2003
Accepted June 14, 2003

IE0209576